Int. J. Heat Mass Transfer. Vol. 33, No. 8, pp. 1649–1666, 1990
Printed in Great Britain

0017-9310/90 $3.00 + 0.00
Pergamon Press plc

Thermocapillary steady and periodic flows in a horizontal layer much thicker than the boundary layer at the free surface

A. G. KIRDYASHKIN, V. F. ZAPOROZHKO and S. P. POPOV
Institute of Geology and Geophysics, Siberian Branch of the U.S.S.R. Academy of Sciences, Novosibirsk, 630090, U.S.S.R.

(*Received* 30 *December* 1988)

Abstract—This paper presents the results of an experimental investigation of thermocapillary and thermogravitational flows in a horizontal layer much thicker than the hydrodynamic boundary layer at the free surface. There is a linear heat source beneath the free surface and a heat sink at the opposite vertical face. At a constant heat flux, boundary layers develop at the free horizontal and the cooling vertical surfaces. Velocity and temperature profiles measured in the boundary layers are presented. Analytical solutions are obtained for the boundary layer at the cooling surface and beyond the boundary layers. The patterns of periodic thermocapillary flows for periods shorter than 24 s are studied: the actual and mean temperatures, the actual and mean values of the friction coefficient at the free surface, the variance of temperature fluctuations, space–time correlation functions, and the boundaries of the propagation of periodic flows.

INTRODUCTION

THERMOCAPILLARY and thermogravitational flows originate in a horizontal layer at any horizontal temperature gradient, however low it may be. The relationship between thermocapillary and thermogravitational forces in a plane-parallel flow (the mode of heat conduction [1]) can be characterized by the complex $k = Ma/Ra = b/\beta\rho g l^2$. With an increase in the layer thickness the effect of the thermocapillary forces on the total flow in the layer decreases.

In different modes of flow, when, for instance, boundary layers get organized, the interaction between these forces is more complex and shows up near the free surface of the liquid.

The interaction between thermocapillary and thermogravitational forces can be expected to be still more complex in unsteady-state modes of flow. The surface thermocapillary forces caused by the reduction of the surface tension with increasing temperature have the nature of molecular interactions and are less persistent as compared with mass thermal gravitational forces.

Kirdyashkin [1] presented an experimental investigation of the pattern of periodic thermocapillary flows originating due to periodic variations in the heat loading on the linear source at the free surface of the liquid. The periodic flows develop in the plane horizontal layer with adiabatic horizontal surfaces. Instantaneous and mean temperature gradients along the free surface and, hence, the friction on the surface, were measured. The boundaries of the propagation of periodic perturbations depending on the amplitude and period of the loading variations were found. It is shown that with $t_0 < 35$ s the thermogravitational forces do not have any appreciable effect on the periodic flow propagation along the surface. The survey of studies of horizontal flows in a horizontal temperature gradient is given in refs. [1, 2].

In the present paper the results of considering experimentally thermocapillary and thermogravitational flows in a horizontal liquid layer are given for the following conditions.

(1) A thermal and hydrodynamic structure in the layer which is much thicker than the hydrodynamic boundary layer at the surface at a steady heat flux (the heat source is located at the surface; the cooling occurs near the opposite vertical face).

(2) The structure of the periodic thermocapillary flows when $t_0 < 24$ s; the actual and averaged temperature fields; the actual and averaged velocity gradients at the surface and, consequently, the friction coefficients; the second order moments (temperature variance, space–time correlation functions); the boundaries of propagation of periodic flows.

The study of the structure of thermocapillary periodic flows is of interest in connection with the prospect of obtaining high-quality materials and single crystals.

EXPERIMENTAL FACILITY AND MEASURING TECHNIQUES

The thermocapillary periodic flows were investigated in a volume of 96% ethyl alcohol of length $x_1 = 370$ mm, height $L = 105$ mm and width $z_1 = 150$ mm with a free adiabatic surface of the liquid. The set-up arrangement and the boundary conditions effected

NOMENCLATURE

a	thermal diffusivity
b	temperature coefficient of surface tension
c_p	heat capacity at constant pressure
g	gravitational acceleration
L	height of a layer
Ma	Marangoni number
$\bar{Q}$	mean value of heat flux for the period
$R(\Delta n, \tau)$	space–time correlation function
$R(\tau)$	autocorrelation function
Ra	Rayleigh number
t	time
t_0	period of heat flux fluctuation
T	temperature
T_c	temperature of vertical cooling surface
T_n	temperature in layer core
T_0	temperature of free surface
u	horizontal velocity component
v	vertical velocity component
x_0	distance of propagation of periodic flows
y, x, z	vertical and horizontal coordinates.

Greek symbols

β	coefficient of thermal expansion of liquid
μ, ν	dynamic and kinematic viscosities
ρ	density
σ	coefficient of surface tension
τ	time shift
τ_0	coefficient of friction at the free surface.

Subscripts and superscript

max	maximum
n	parameter of layer core
0	free surface of liquid
$\bar{}$	mean value.

in the experiment are given in Fig. 1. The experimental set-up, the construction of which is presented in detail in ref. [1], was made of optically transparent organic glass.

As a periodic heat source, use was made of a nichrome filament, 0.15 mm in diameter and 145 mm in length, stretched between two rigid holders. The nichrome filament was arranged horizontally at a distance of 5 mm from the vertical thermally insulated face and at a distance of 0.2–0.3 mm from the free surface.

The control system for a periodically alternating heat flux is given in ref. [1]. The heat source power can be regulated by the law

$$Q = Q_1 + \bar{Q}_1\left(1+\sin\frac{2\pi t}{t_0}\right),$$

where $0.2\ \text{s} < t_0 < 100\ \text{s}$.

The amplitude of the heat flux power was regulated within the range 0–45 W.

The constancy of the cooling vertical brass surface temperature T_c was ensured by pumping thermostatically regulated water through the inner cavity of the heat exchanger, the time averaged temperature of which was maintained within ± 0.05°C.

The temperature of the liquid in the boundary layer at the vertical cooling heat transfer surface was measured with a nichrome–constantan microthermocouple made of 0.05 mm diameter wires. The working portion of the needle-type thermocouple extended 10 mm from the glass holder and was set parallel to the surface. The other junction of the thermocouple was maintained at the ice melting temperature. With the aid of a macroscrew, the thermocouple was traversed horizontally and vertically. Its vertical position was determined accurate to 0.01 mm

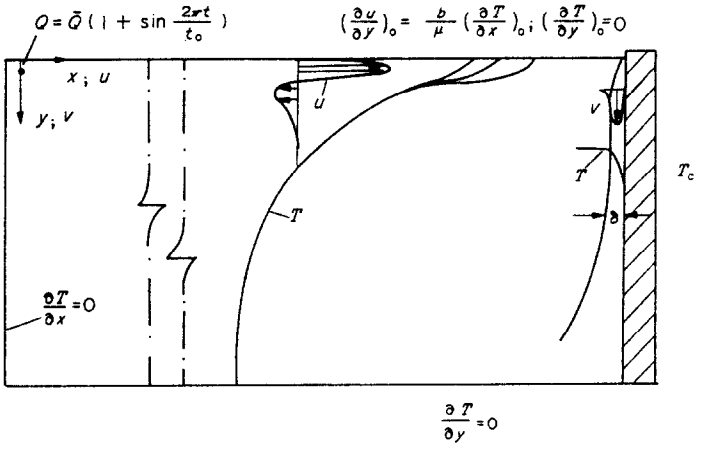

FIG. 1. Flow pattern and boundary conditions in studying periodic flows.

by using a V-630 cathetometer. The thermocouple traversed along the coordinate 'x' normal to the cooling wall and was fixed by a clock-type indicator with 2 μm division. The initial position of the thermocouple junction (a contact with the wall) was indicated by the V-630 cathetometer and thereupon was refined when constructing the temperature distribution across the boundary layer: the point was determined at which the linear temperature distribution in the wall boundary layer intersected with the constant temperature line, which corresponded to the local wall temperature.

The temperature gradient on the free surface of the liquid was measured using a differential microthermocouple and fixed in the form of an analogous signal. Its value was found from the formula

$$\partial T/\partial x = U_t/KR\Delta x$$

where U_t is the amplified part of the differential thermocouple e.m.f., K the amplification factor of the system based on the loaded resistance equivalent to that of the thermocouple, R the thermocouple sensitivity (μV °C^{-1}), and x the spacing between the junctions of the differential thermocouple.

The constructions of probes and the techniques of measuring temperature and velocity in the ethyl alcohol layer were similar to those employed in ref. [1]. The only differences were in the methods of fixing instantaneous e.m.f.s of the microthermocouple, which were measured with the aid of a digital voltmeter (with a sensitivity of 1 μV), which was also an analogue-to-digital converter. After passing the matching device of the KAMAK system, the voltmeter signals were put into storage and pressed by the dialogue computing complex DVK-2M.

Instantaneous local temperature drops in the layer relative to the temperature of the thermostatically regulated water, which cooled the heat exchanger, were found from the formula $T(t) = U_t/R$, where U_t is the measured e.m.f. of the thermocouple. Discrete realizations of instantaneous temperature drops $T(t)$ were recorded at the time instants $t_i = ih$ ($i = 1, 2, \ldots, N$), where $h = 1/f_b$ is the discretization step and f_b is the discretization frequency. The frequency of selection of the thermocouple e.m.f.s and the file of numerical data $N = 1024$ were specified by the programme. The following random statistic characteristics of the discretized realizations of instantaneous local temperature drops were calculated: the mean values $\bar{T} = \Sigma_{i=1}^{N} T_i/N$; instantaneous temperature fluctuations $T'(t) = T(t) - \bar{T}$; the qth central moment $m_q = [\Sigma_{i=1}^{N}(T_i - \bar{T})]q/N$, $q = 2, 3, 4$; the variance $m_2 = \overline{T'^2}$; the autocorrelation function $R(\tau) = T'(t) \cdot T'(t+\tau)/R(0)$; the space correlation function $R(\Delta n; \tau) = T'_1(t) \cdot T'_2(t+\tau)/[R_1(0) \cdot R_2(0)]^{1/2}$ where τ is the time shift; $T'_1(t)$ and $T'_2(t)$ the temperature values on the first and second probes, Δn the spacing between the probes along the x- or y-axis; the microscale of the time τ_ξ determined from the equation of the parabola which approximates $R(\tau)$ in the vicinity of $\tau = 0$, $R(\tau) = 1 - \tau^2/\tau_\xi^2$.

RESULTS OF MEASUREMENTS AND THEIR ANALYSIS

Constant heat flux

At a constant heat flux from a cylindrical heater (a filament) and under the boundary conditions in the liquid layer indicated in Fig. 1, there exist two boundary layers: at the horizontal free and cooling vertical surfaces. The horizontal temperature gradient gives rise to the thermocapillary forces

$$\tau_0 = \frac{d\sigma}{dT}\left(\frac{\partial T}{\partial x}\right)_0$$

on the free surface. For ethyl alcohol $d\sigma/dT = b = 9 \times 10^{-5}$ N m^{-1} deg^{-1}.

The boundary layer flow at the free surface results from the interaction of thermocapillary and thermogravitational forces.

Under the conditions of thermal and thermocapillary convection, the equations for the boundary layer at the horizontal surface have the form

$$\frac{\partial^2 u^2}{\partial x \partial y} + \frac{\partial^2 uv}{\partial y^2} = \beta g \frac{\partial T}{\partial x} + \nu \frac{\partial^3 u}{\partial y^3} \tag{1}$$

$$\frac{\partial uT}{\partial x} + \frac{\partial vT}{\partial y} = a \frac{\partial^2 T}{\partial y^2} \tag{2}$$

$$\frac{\partial u}{\partial x} + \frac{\partial v}{\partial y} = 0. \tag{3}$$

The boundary conditions on the free surface ($y = 0$) are

$$\left(\frac{\partial u}{\partial y}\right)_0 = \frac{1}{\mu}\frac{d\sigma}{dT}\left(\frac{\partial T}{\partial x}\right)_0; \quad v = 0; \quad \frac{\partial T}{\partial y} = 0 \tag{4}$$

at $x = x_1$ and $T = T_1$. The conditions at the edge of the boundary layer can be elucidated if the laws governing temperature variations in the layer core are known. The layer core is understood to be the area beyond the boundary layers.

In the layer core, any horizontal gradient, however small, may give rise to horizontal flows which equilibrate the temperature along the x-axis. For these large-scale motions the viscosity forces are vanishingly small.

For the layer core under steady-state conditions, it is possible to assume in the first approximation that the temperature in the horizontal section is constant, i.e. the horizontal flow velocity is negligible [2].

Within the scope of this assumption, the temperature field $T_n(y)$ is formed in the layer core.

Heat removal is affected by the vertical cooling surface, at which a free-convective boundary layer is formed, with the flow in it being directed downward. An oppositely directed flow (v_n) should exist in the

core of the layer. It can be assumed that in the layer core v_n = const., since $v_n(y)$ horizontal flows can occur which, in the presence of the cooling vertical surface, can give rise to a horizontal temperature gradient in the layer core. Thus, the assumption that $T_n(y)$ yields v_n = const. in the layer core is valid.

The layer core is described by the equation:

$$v_n \frac{\partial T_n}{\partial y} = a \frac{\partial^2 T_n}{\partial y^2}. \tag{5}$$

Under the boundary conditions: $y = 0$, $T = T_m$; $y = \infty$, $T = 0$ the solution of equation (5) has the form

$$T_n = T_m \, e^{v_n y/a} \tag{6}$$

where $v_n < 0$.

The temperature distribution occurring in the layer core and corresponding to equation (6) is presented in Figs. 2 and 3. This correspondence indicates that v_n = const. in the layer core.

Thus, in the outer part of the thermal boundary layer at the free surface, the temperature varies by law (6) and the heat flux at the edge of the boundary layer is equal to zero; the normal velocity component is v_n = const. and the longitudinal component is $u = 0$. Near the heater the temperature gradient along the surface can attain large absolute values, and the thermocapillary forces are much larger than the thermogravitational forces; as $|\partial T/\partial x|_0$ decreases away from the heater, the thermogravitational forces become predominant.

Consideration will be given to the free-convective boundary layer at the cooling vertical plate located in the vertical section $x = x_1$. The origin of the coordinates will be taken as follows: the y-axis is oriented vertically downward from the free surface and the x-axis—normally to the vertical surface.

The solution of the thermal boundary layer on the cooling vertical surface is presented in the form [3]:

$$T = T_n(y) + \theta(x; y). \tag{7}$$

Then the boundary layer equation has the form

$$v \frac{\partial T_n}{\partial y} + v \frac{\partial \theta}{\partial y} + u \frac{\partial \theta}{\partial x} = a \frac{\partial^2 \theta}{\partial x^2}. \tag{8}$$

In the case considered, $v\theta < vT_n$ and the second term of equation (8) can be neglected. Taking into account that $u \ll v$, the term $u(\partial\theta/\partial x)$ can also be neglected. Equation (8) will then take on the form

$$v \frac{\partial T_n}{\partial y} = a \frac{\partial^2 \theta}{\partial x^2}. \tag{9}$$

Since the inertia terms can be disregarded owing to their smallness, the equation of the dynamic boundary layer at the vertical wall can be written under the Boussinesq approximation as

$$v \frac{\partial^2 v}{\partial x^2} = \beta g \theta. \tag{10}$$

The boundary conditions for equations (9) and (10) are

$$x = 0: \quad v = 0, \ \theta = \theta_1 \left(\text{or} \quad \frac{\partial \theta}{\partial x} - \theta'_1 \right);$$

$$x = \infty: \quad v = 0, \ \theta = 0. \tag{11}$$

The magnitude of the velocity v_n is obtained from the

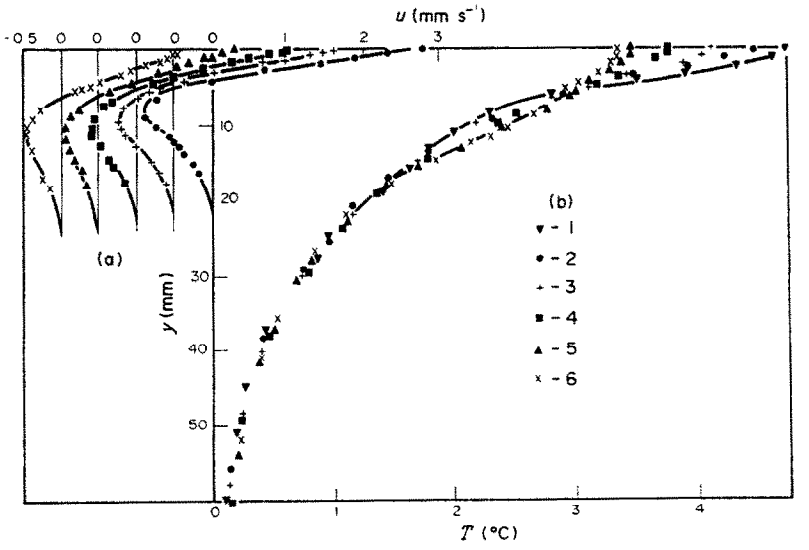

FIG. 2. (a) Profiles of the longitudinal velocity component (u) at the free surface of ethyl alcohol. (b) Temperature profiles over the layer height L = 105 mm, x_1 = 370 mm and z_1 = 150 mm at Q = 17 W m^{-1} and at different distances from the heater: 1, x = 28 mm; 2, x = 60 mm; 3, x = 100 mm; 4, x = 170 mm; 5, x = 240 mm; 6, x = 280 mm.

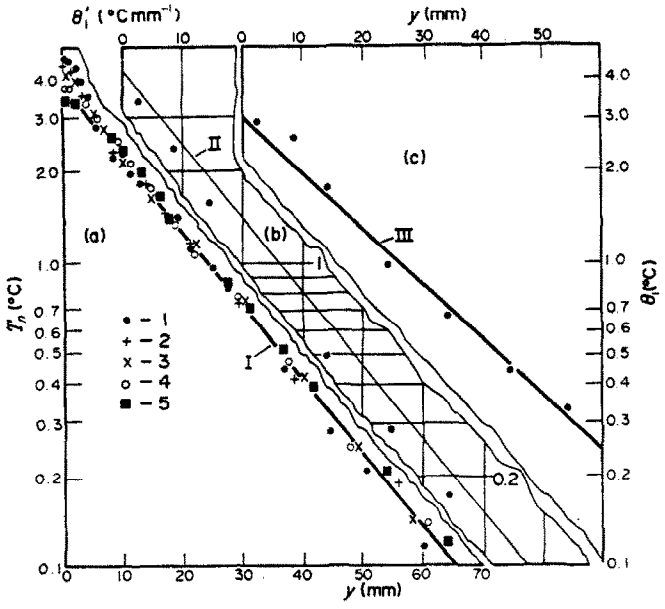

FIG. 3. (a) Temperature profiles over the layer height $L = 105$ mm, $x_1 = 370$ mm for $Q = 17$ W m^{-1} and different values of x: 1, $x = 28$ mm; 2, $x = 60$ mm; 3, $x = 100$ mm; 4, $x = 170$ mm; 5, $x = 240$ mm. I, By equation (23). (b) The temperature gradient $\partial\theta/\partial x$ at the cooling surface vs the y-axis. II, By equation (24). (c) Temperature variations of the cooling surface over the height (y). III, By equation (25).

equation

$$v_n = \frac{1}{x_1}\int_0^{\delta} v(x)\,dx. \tag{12}$$

Since $\delta \ll x_1$, then $v \gg v_n$ and for $x \gg \delta$ it is possible to assume that $v = 0$.

Equation (10) is differentiated twice with respect to 'x' and substituted into equation (9)

$$\frac{\partial^4 v}{\partial x^4} + v\frac{\beta g}{av}\left(-\frac{\partial T_n}{\partial y}\right) = 0. \tag{13}$$

Let

$$4m^4 = \frac{\beta g}{av}\left(-\frac{\partial T_n}{\partial y}\right). \tag{14}$$

Since $\partial T_n/\partial y < 0$, then $4m^4 > 0$. The general form of the solution for the equation $(D^4+4m^4)v = 0$ at $v(0) = 0$ and $v(\infty) = 0$ is

$$v = c \cdot \sin mx \cdot e^{-mx}. \tag{15}$$

Under the boundary conditions (11) and $\theta(0) = \theta_1$, the solutions of equations (9), (10) and (12) are

$$v = -\frac{\beta g\theta_1}{2vm^2} e^{-mx} \sin mx \tag{16}$$

$$\theta = \theta_1 e^{-mx} \cos mx \tag{17}$$

$$v_n = \frac{\beta g\theta_1}{4vm^3 x_1}; \quad \theta = \frac{v_n}{a}\frac{4vam^3 x_1}{\beta g}. \tag{18}$$

Under the boundary conditions (11) and $\partial\theta/\partial x = \theta'_1$ at $x = 0$, the solution of the system of equations (9), (10) and (13) will yield

$$v = \frac{\beta g\theta'_1}{2vm^3} e^{-mx} \sin mx \tag{19}$$

$$\theta = -\frac{\theta'_1}{m} e^{-mx} \cos mx \tag{20}$$

$$v_n = -\frac{\beta g\theta'_1}{4vx_1 m^4}, \quad \theta'_1 = \frac{v_n x_1}{a}\frac{\partial T_n}{\partial y}. \tag{21}$$

As follows from equations (15), (18) and (21), the condition $v_n = \text{const.}$ will be fulfilled when

$$\theta_1 \sim \left(\frac{\partial T_n}{\partial y}\right)^{3/4} \quad \text{and} \quad \theta'_1 \sim \frac{\partial T_n}{\partial y}. \tag{22}$$

The validity of the adopted approximations, namely the uniformity of temperature of the horizontal plate for the layer core, the constancy of the velocity v_n in the layer core and the correctness of approximations in solving the equations of the boundary layer at the cooling surface, is assessed experimentally.

Experimental investigations were conducted in the ethyl alcohol layer of height $L = 105$ mm, length $x_1 = 370$ mm and width $z_1 = 150$ mm at a steady heat flux on the filament $Q = 22$ W m^{-1}. The results of the measurements are given in Figs. 2–4. Near the free surface, there exists a laminar boundary layer with the thickness much smaller than that of the liquid layer. Under the conditions of steady stratification, there originate oppositely directed flows. The change of temperature along the surface gives rise to the

thermocapillary forces on the free surface (Fig. 2). The thermal boundary layer is also considerably thinner than the liquid layer; the temperature in the layer core varies only along the coordinate 'y' and stable stratification over the height of the entire liquid layer is observed (Fig. 2). Near the cooling vertical surface, a free-convective boundary layer develops (Fig. 4).

In solutions (16)–(21) the unknown parameter is the velocity v_n. The determination of v_n involves the closure of the solutions for the boundary layer at the horizontal free surface and for the boundary layer at the vertical cooling surface, the solution for the boundary layer at the free surface not being obtained. Therefore, the velocity v_n will be found from the experimental temperature distribution over the layer height (Fig. 2 (b)).

According to the experiments (Figs. 2(b) and 3(a)), the temperature distribution over the layer height can be approximated by exponential relation (6)

$$T_n = 3.8\,e^{-55.24y}. \tag{23}$$

It follows from equations (6) and (23) that $v_n/a = -55.24\ \text{m}^{-1}$ and, consequently, $v_n = -4.955 \times 10^{-6}\ \text{m s}^{-1}$ at $T = 25°\text{C}$. The ratio v_n/a being known, the laws governing the cooling surface temperature variations θ_1 and the temperature gradient θ_1' at this surface can be obtained from equations (18) and (21).

Figure 3(b) presents comparison of the values of the temperature gradient at the cooling surface calculated by equation (21)

$$\theta_1' = 4290\,e^{-55.24y}\quad (°\text{C m}^{-1}) \tag{24}$$

with those determined experimentally. A satisfactory agreement of the predicted and experimental data is observed.

The experimental values of the cooling surface temperature correspond to the distribution of θ_1 predicted by equation (18) in terms of the known quantity v_n/a

$$\theta_1 = 2.96\,e^{-41.43y}\quad (°\text{C}) \tag{25}$$

as follows from Fig. 3(c). The comparisons given indicate the validity of relations (22).

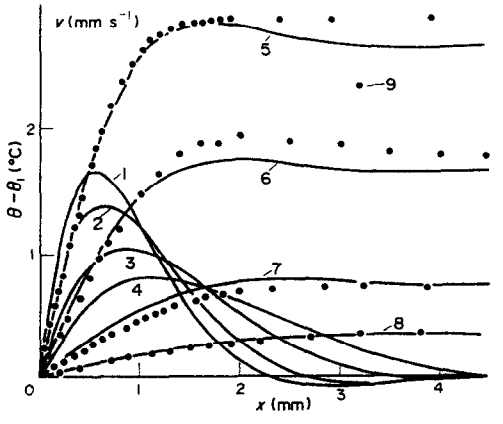

FIG. 4. The profiles of the velocity v in the boundary layer at the cooling surface at different values of y by equation (16) or (19): 1, $y = 2.58$ mm; 2, $y = 14.24$ mm; 3, $y = 33.8$ mm; 4, $y = 54.4$ mm. Temperature profiles by equation (17) or (20): 5, $y = 2.58$ mm; 6, $y = 14.24$ mm; 7, $y = 33.8$ mm; 8, $y = 54.4$ mm. 9, experimental values of temperature.

Figure 4 presents a comparison of the experimental temperature profiles and those determined theoretically following solution (17) or (20) at the known value of v_n/a. A good agreement of theory and experiment is observed (Fig. 4). The figure also gives theoretical velocity profiles at the cooling surface predicted by equations (16) and (19).

Thus, the assumptions on the hydrodynamics and heat transfer in the layer core and the cooling surface adopted in solving the problem are quite permissible and allow an analytical estimate of the behaviour of thermal gravitational flows in these regions.

From the temperature and velocity profiles measured experimentally over the layer height, it is possible to determine the heat flux directed horizontally

$$Q = c_p \rho \int_0^{\delta} uT\,dy.$$

According to the measured velocity and temperature profiles at $x = 170$ mm, $Q = 17\ \text{W m}^{-1}$, which is 30% smaller than the heat flux of $22\ \text{W m}^{-1}$ supplied to the filament.

The difference between the heat fluxes is associated with heat losses through the lateral faces and through the upper air layer. These losses (30%) could not be avoided. The greatest heat losses are to be expected in the vicinity of the heater, where the temperature gradients are maximal. The same heat losses were also observed at the heat flux alternating periodically on the horizontal filament.

Periodic flows at $t_0 = 3$ s

The structure of periodic flows was considered in the absence of the constant component of the heat flux Q_1

$$Q = \tilde{Q}\left(1 + \sin\frac{2\pi t}{t_0}\right) \tag{26}$$

and when $3\ \text{s} \leqslant t_0 \leqslant 24$ s. The working volume was filled with 96% ethyl alcohol and the heater, i.e. a nichrome wire, was immersed to a depth of 0.2–0.3 mm from the free surface. When the filament is located near the surface and Q is maximum, the liquid near the heater becomes superheated and evaporates. The measurements were performed over a period of 3.5 h after the periodic heat flux had been supplied.

The experimental results obtained for $t_0 = 3$ s, $L = 105$ mm, $x_1 = 370$ mm, $z = 150$ mm, $\tilde{Q} = 22\ \text{W m}^{-1}$, $T_c = 21.7°\text{C}$ and $f_b = 10$ Hz are given in Figs. 5–16. The free surface temperature was measured by two thermocouples, one of them fixed and the other moving along the x-axis, while remaining in the same plane $z = \text{const}$. The cold junctions of the thermo-

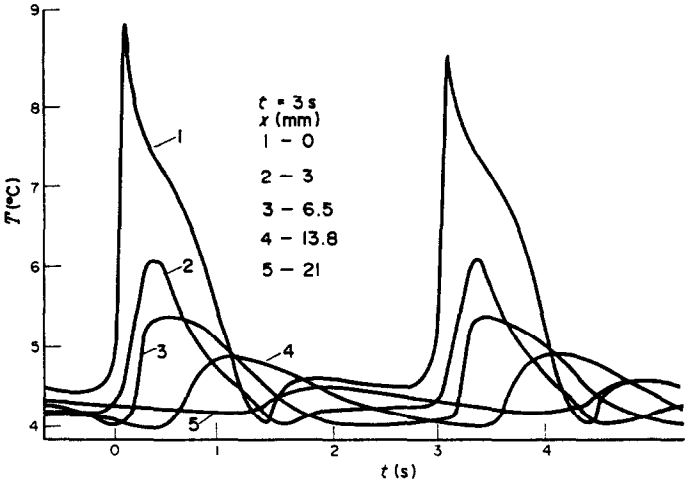

FIG. 5. Variations of the free surface temperature in time for different distances (x) from the heater in the layer $L = 105$ mm, $x_1 = 370$ mm, $\bar{Q} = 22$ W m^{-1}, $T_c = 21.7$°C, $t_0 = 3$ s.

couple had the temperature of the thermostatically regulated cooling water, which circulated in the cavity of the vertical heat exchanger. In such a manner instantaneous temperature drops in the layer were measured with respect to the temperature in the vicinity of $y = L$ and, consequently, with respect to the cooling surface of the copper vertical heat exchanger at y values greater than the boundary layer thickness at the free surface near the cooler.

Figure 5 presents instantaneous values of the free surface temperature at different distances from the periodic heat flux source and the phase shift at different values of 'x'. The temperature varies in time periodically at different x values, decreasing in amplitude during removal from the heater. The amplitude and the mean temperature for different values of 'x' are given in Fig. 6. From the plots of Figs. 5 and 6, instantaneous temperature values can be found for different values of t/t_0 and x.

Figure 7 illustrates phase shift-induced variations in the maximum temperature t_ϕ/t_0 at different values of x and the phase rate of the maximum temperature u_ϕ. The resolving power of temperature measurements made it possible to trace the phase shift up to $x = 25$ mm, in this case $t_\phi/t_0 = 0.7$, and the amplitude of temperature fluctuations amounted to 0.05 T.

When 5 mm $< x <$ 25 mm, the mean temperature gradient along the surface in the periodic flow region is small in magnitude and varies monotonously ($\partial \bar{T}/\partial x < 0$).

Measurements were taken directly of the instantaneous values of the temperature gradient $(\partial T/\partial x)_0$ on the free surface and the mean values $(\overline{\partial T}/\partial x)_0$ were determined.

The friction coefficients due to the thermocapillary forces and velocity gradients normal to the surface were respectively obtained from the relations

$$\frac{\tau_0}{\rho} = \nu\left(\frac{\partial u}{\partial y}\right)_0 = \frac{1}{\sigma}\frac{d\sigma}{d\bar{T}}\left(\frac{\partial \bar{T}}{\partial x}\right)_0. \qquad (27)$$

Their values on the free surface vary periodically in time at different distances from the heater (Fig. 8). When $x < 22$ mm, the change takes place in the sign of the quantity $(\partial T/\partial x)_0$ for the period of fluctuation and, consequently, in the direction of the thermocapillary force vector. The mean value of the friction coefficient is always $\bar{\tau}_0 < 0$ (Fig. 9).

Figure 10 presents the autocorrelation functions of temperature fluctuations on the free surface. At different distances from the heater, the autocorrelation function varies rigorously periodically. As follows from the space correlation function (Fig. 11), the temperature fluctuations along the free surface are periodical in character, the phase shift being less than the fluctuation period of the heat flux.

The temperature alternates periodically in time at different distances from the free surface (Figs. 12(a) and (b)); near the surface an inconsiderable tem-

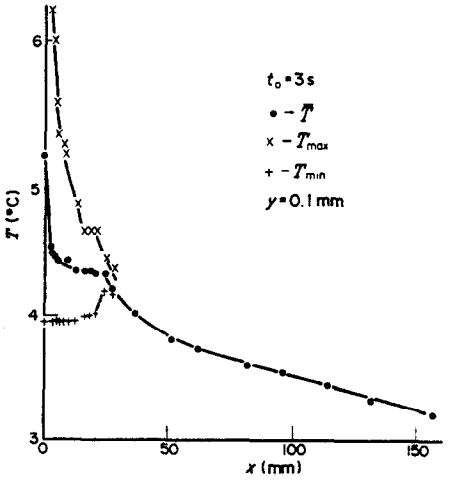

FIG. 6. The maximum (T_{max}), mean ($\bar{T}$) and minimum (T_{min}) periodic temperature fluctuations on the free surface vs 'x' ($t_0 = 3$ s).

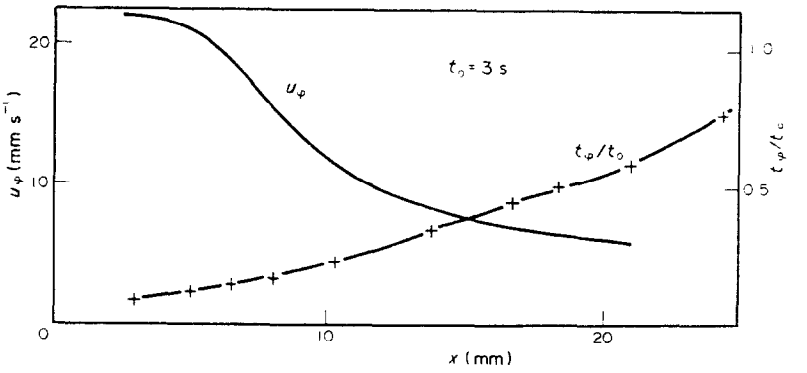

FIG. 7. The phase shift and phase velocity of the maximum temperature on the free surface vs 'x' (t_0 = 3 s).

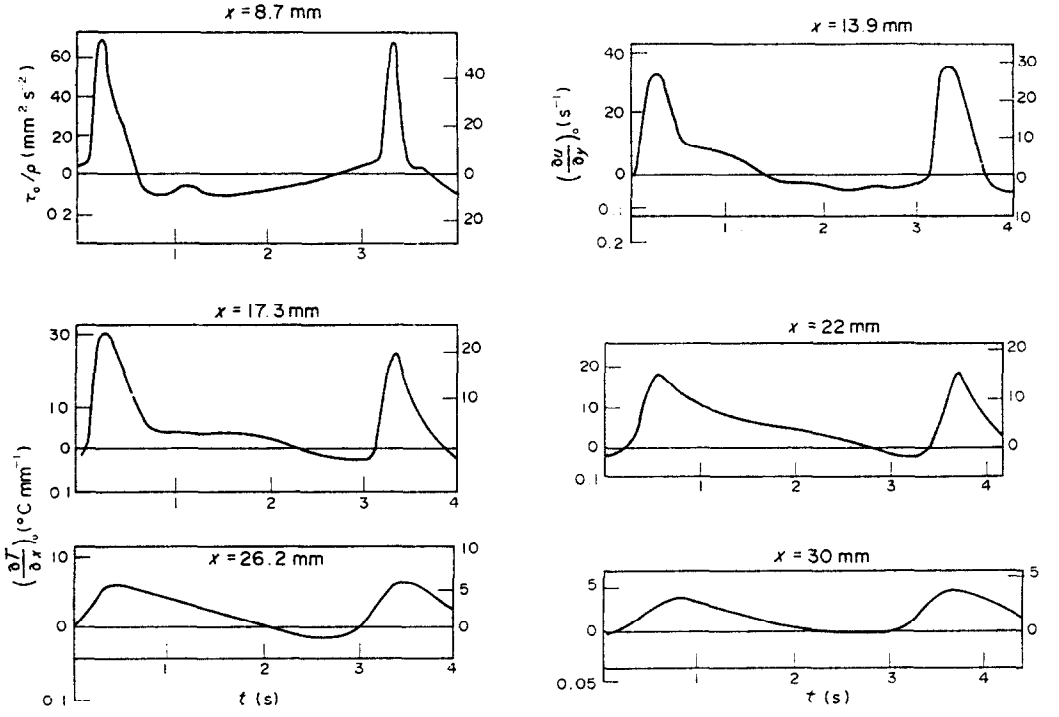

FIG. 8. The longitudinal temperature gradient $(\partial T/\partial x_0)_0$, the velocity gradient $(\partial u/\partial y)_0$ and the friction τ_0/ρ on the free surface for different values of x (t_0 = 3 s).

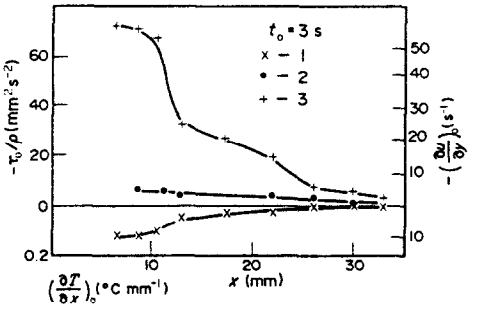

FIG. 9. The maximum (1), mean (2) and minimum (3) values of τ_0/ρ, $(\partial u/\partial y)_0$ and $(\partial T/\partial x)_0$ on the free surface (t_0 = 3 s).

perature gradient is observed (Fig. 13). The mean-square temperature fluctuations vary at the free surface (Fig. 13).

The autocorrelation functions (Fig. 14) and the space correlation functions of the temperature fluctuations (Fig. 15) over the boundary layer thickness are periodic in character and are correlated with respect to the coordinate y.

The measurements of velocity and temperature profiles in the region of the developed flow show that the value of the temperature gradient along the free surface is constant (Fig. 6) and, hence, the velocity on the free surface is also constant (Fig. 16). It should be

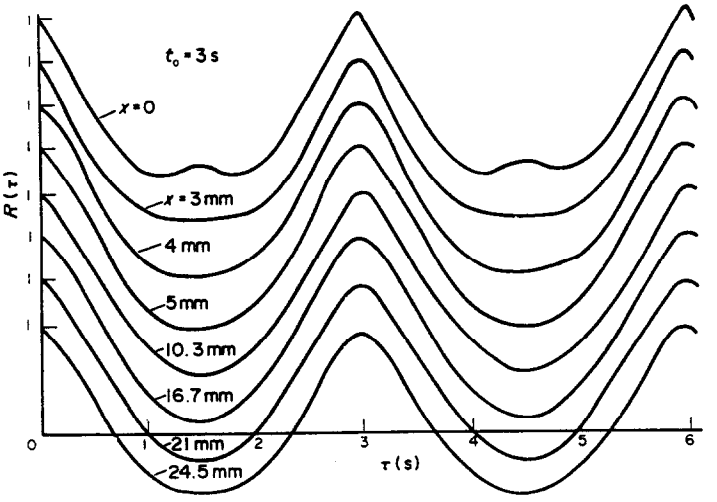

FIG. 10. The autocorrelation functions of temperature fluctuations on the free surface at different distances from the heater ($t_0 = 3$ s).

noted that, due to the periodic boundary layer flow near the heat source, the flow develops under conditions differing from those of the steady heat flux (Fig. 2). At the periodic heat flux, the effective value of x is greater than that at the steady heat flux equal to the mean value $\bar{Q}$. In the region of the developed flow at $x = 150$ mm, the horizontally directed heat flux calculated from the measured velocity and temperature profiles appeared to be 30% lower than the mean heat flux supplied to the heater, i.e. to be equal to 17 W m^{-1}. This means that the heat flux varies with distance from the heater. However, it was impossible to measure the values of the heat flux in different vertical sections of the periodic layer.

Periodic flows at $t_0 = 12$ s

The experimental results obtained for the regime $t_0 = 12$ s, $L = 105$ mm, $x_1 = 370$ mm, $z_1 = 150$ mm, $\bar{Q} = 22$ W m^{-1}, $T_c = 21.7$°C and $f_b = 5$ Hz are presented in Figs. 17–26. The periodic temperature fluctuations at the free surface for $t_0 = 12$ s and $x < 11$ mm (Fig. 17) are more complex in character than those for $t_0 = 3$ s (Fig. 5). The phase shift for the lifetime of an individual periodic flow is commensurable with the fluctuation period of the heat flux (Fig. 17). The mean free surface temperature diminishes with distance from the heater; in the developed flow region the quantity $\bar{T}$ changes linearly with x (Fig. 18).

The autocorrelation functions of temperature fluctuations on the free surface for different values of x are of periodic character (Fig. 19). It follows from the space correlation functions (Fig. 20) that the time shift τ_{max}, at which the greatest correlation coefficient $R(\Delta n, \tau)$ is observed for Δn comparable with x_0, is smaller than the fluctuation period of the heat flux;

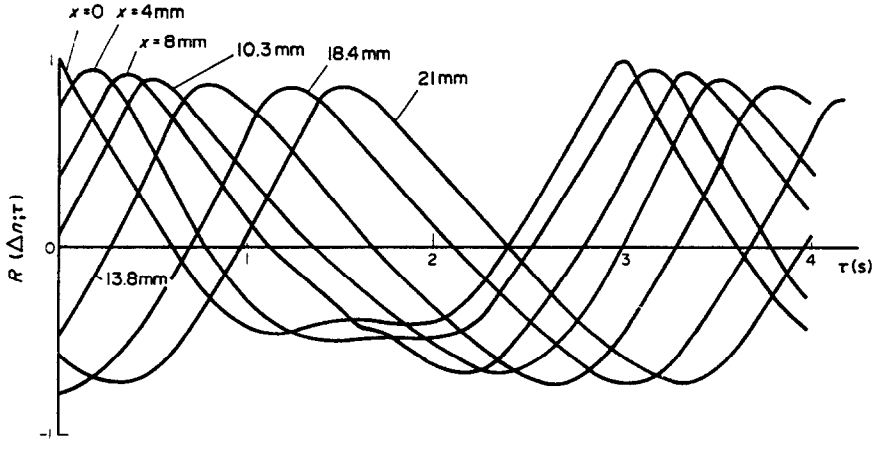

FIG. 11. The space–time correlation functions of temperature fluctuations on the free surface for different shifts $\Delta n = x$ ($t_0 = 3$ s).

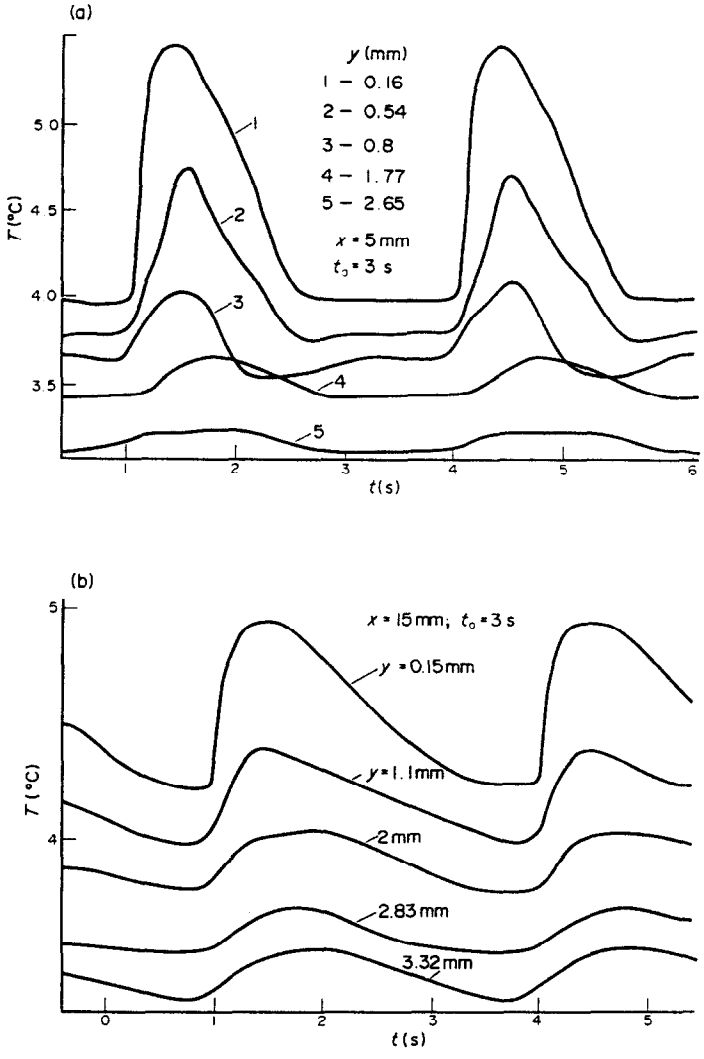

FIG. 12. Temperature variations in time for different values of y at $t_0 = 3$ s. (a) $x = 5$ mm. (b) $x = 15$ mm.

the greatest correlation coefficient for the temperature fluctuations on the free surface varies little with an increase in the shift Δn; based on the time shift for the fixed spatial shift τ_{max}, it is possible to assess the velocity of temperature perturbation on the free surface of the liquid $\Delta n/\tau_{max}$.

The friction coefficients τ_0 and $(\partial u/\partial y)_0$ due to the thermocapillary forces are calculated from equation (27) and from the values of $(\partial T/\partial x)_0$ determined for different values of x (Fig. 21). The friction coefficients vary periodically with time (Fig. 21) and when $15 < x < 40$ the flows directed toward the heater appear on the free surface.

However, the mean values of τ_0 and $(\overline{\partial u}/\partial y)_0$ vary monotonously without changing their sign, and the mean velocity of the free surface is always positive (Fig. 22).

The temperature fluctuations over the layer thickness were measured for the sections $x = 9$ mm (Fig. 23(a)) and $x = 25$ mm (Fig. 23(b)). With the immersion of the thermocouple, the temperature fluctuations become more complex, but are of periodic character (Fig. 23(a)). The mean values of temperature near the surface vary little, indicating the possibility for measuring correctly the free surface

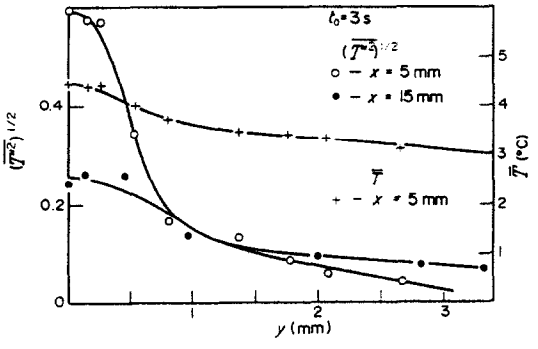

FIG. 13. The mean ($\bar{T}$) and mean-square values of temperature fluctuations over the layer depth 'y' ($t_0 = 3$ s).

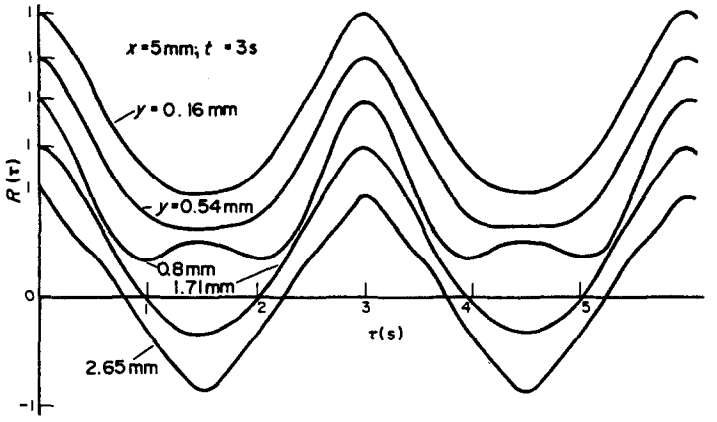

FIG. 14. The autocorrelation functions of temperature fluctuations over the layer depth and $x = 5$ mm ($t_0 = 3$ s).

temperature (Fig. 24). The mean-square temperature fluctuations change non-monotonously with increasing y (Fig. 24). The autocorrelation and space correlation functions of the temperature fluctuations vary strictly periodically with change in the time shift τ (Figs. 25(a), (b) and 26(a), (b)). The temperature fluctuations over the boundary layer thickness are rigidly correlated (Figs. 26(a) and (b)).

The limit of the periodic flow propagation (x_0)

The study of the periodic flow structure shows that the lifetime of an individual periodic flow is com-

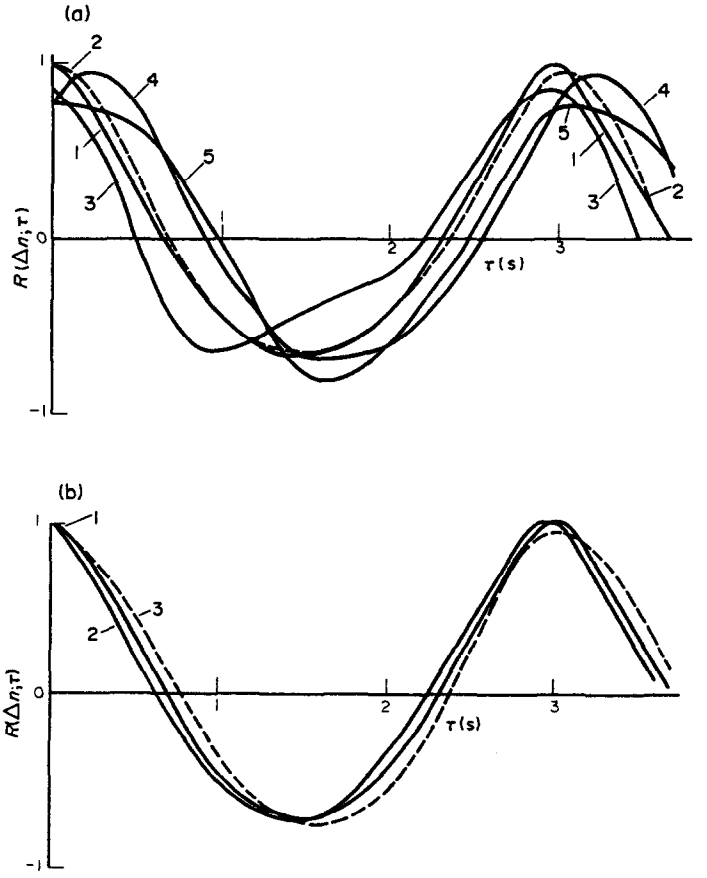

FIG. 15. The space–time correlation functions of temperature fluctuations over the layer depth ($t_0 = 3$ s). (a) $x = 5$ mm, $\Delta n = (y-0.16)$ mm: 1, $y = 0.16$ mm; 2, $y = 0.45$ mm; 3, $y = 0.8$ mm; 4, $y = 1.77$ mm; 5, $y = 2.65$ mm. (b) $x = 15$ mm, $\Delta n = (y-0.15)$ mm: 1, $y = 0.15$ mm; 2, $y = 0.45$ mm; 3, $y = 3.32$ mm.

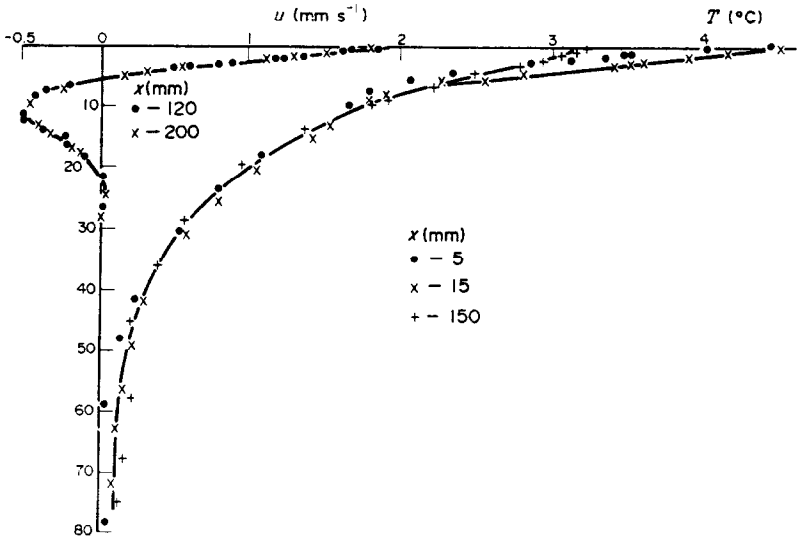

FIG. 16. The velocity and temperature profiles far from a periodically varying heat flux at $t_0 = 3$ s and $Q = 17$ W m^{-1}.

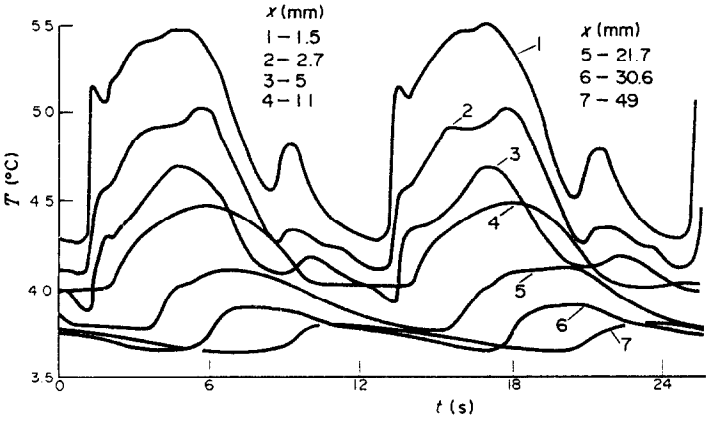

FIG. 17. Variations of the free surface temperature in time for different values of x in the layer $L = 105$ mm, $x_1 = 370$ mm, $\bar{Q} = 22$ W m^{-1}, $T_c = 21.7$°C and $t_0 = 12$ s.

mensurable with the period of heat loading variation. For example, for $t_0 = 3$ s the phase shift of the maximum temperature at $x = 25$ mm comprises $t_\phi/t_0 = 0.7$ and the temperature fluctuation amplitude is equal to $0.05\bar{T}$ (Fig. 5); for $t_0 = 12$ s and $x = 49$ mm the phase shift is $t_\phi/t_0 = 0.7$ and the temperature fluctuation amplitude is $0.04\bar{T}$ (Fig. 17). The same is indicated by the space correlation functions calculated from the experimental data (Figs. 11 and 20): the time shift τ_{max} corresponding to the maximum value of $R(\Delta n, \tau)$ (for Δn comparable with x_0) is smaller than the heat flux fluctuation period (the time shift τ_{max} characterizes the magnitude of the phase shift t_ϕ).

The periodic flow can be assumed to propagate to such a distance x_0 from the heater which is covered by the liquid at the free surface for the time commensurable with the fluctuation period at the heat flux commensurable with the mean value of the latter.

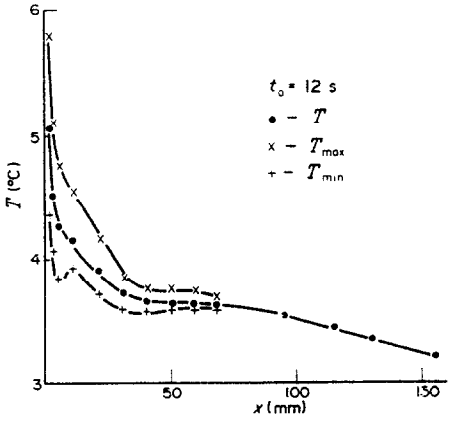

FIG. 18. The maximum (T_{max}), minimum (T_{min}) and mean ($\bar{T}$) periodic temperature fluctuations on the free surface vs 'x' ($t_0 = 12$ s).

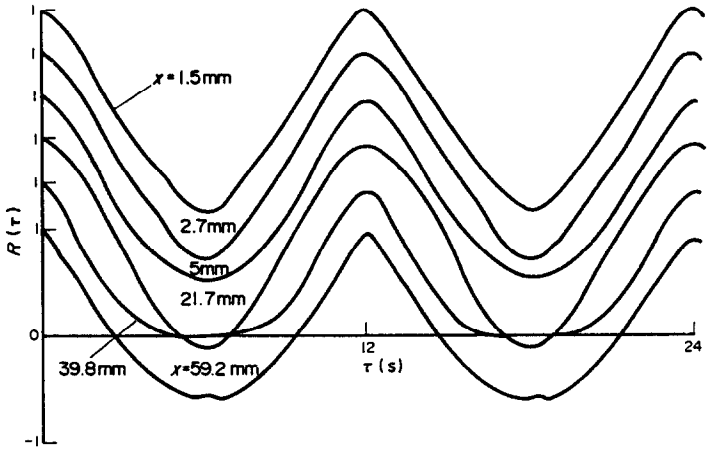

FIG. 19. The autocorrelation functions of temperature fluctuations on the free surface for different values of x ($t_0 = 12$ s).

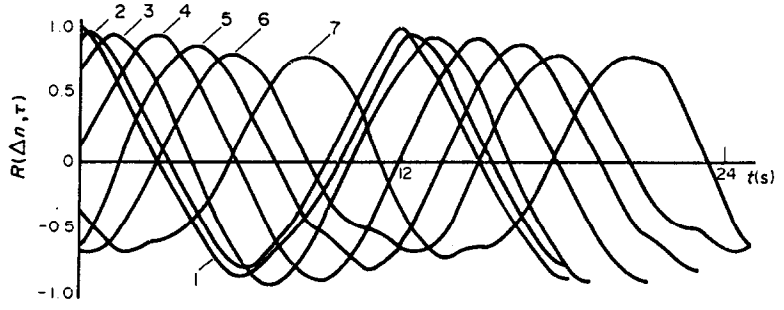

FIG. 20. The space–time correlation functions of temperature fluctuations on the free surface for different shifts: $\Delta n = (x - 1.5)$ mm, $t_0 = 12$ s. 1, $x = 1.5$ mm; 2, $x = 5$ mm; 3, $x = 11$ mm; 4, $x = 21.7$ mm; 5, $x = 30.6$ mm; 6, $x = 39.8$ mm; 7, $x = 59.2$ mm.

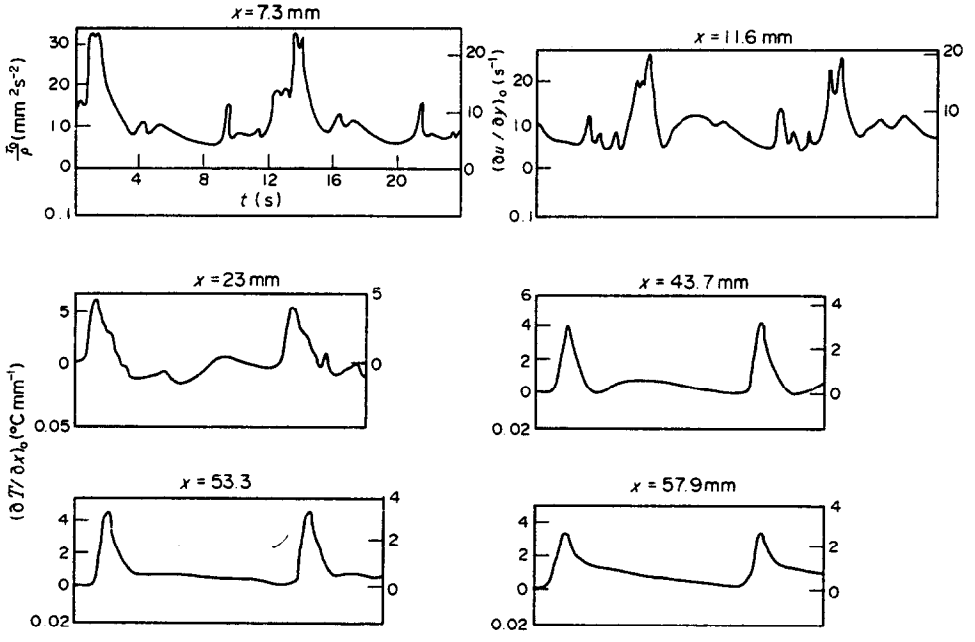

FIG. 21. The longitudinal temperature gradient $(\partial T/\partial x)_0$, the velocity gradient $(\partial u/\partial y)_0$ and the friction τ_0/ρ on the free surface for different values of x ($t_0 = 12$ s).

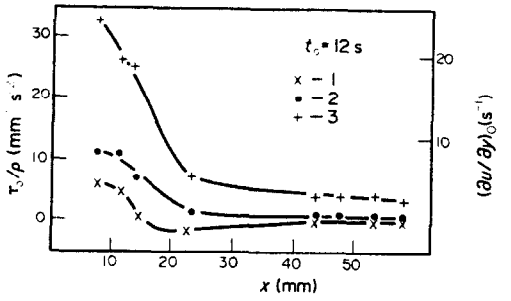

FIG. 22. The maximum (1), mean (2) and minimum (3) values of τ_0/ρ, $(\partial u/\partial y)_0$ and $(\partial T/\partial x)_0$ on the free surface ($t_0 = 12$ s).

In the region of the existence of periodic flow, there exist the greatest temperature gradients along the surface (Figs. 6 and 18) and thermocapillary forces which are much in excess of thermogravitational forces. Therefore, it is possible to set $g = 0$ in equation (1).

Assuming for $y \to \infty$

$$\partial T/\partial y = 0, \quad T(\infty) = \text{const.}, \quad u = v = 0 \tag{28}$$

as the boundary conditions on the outer part of the boundary layer (Q = const.), equations (1)–(3) at $g = 0$ and boundary conditions (4) and (28) can be presented in the form of the differential equations

$$\left.\begin{aligned} 4\phi''' + \phi\phi'' + 2\phi'^2 = 0 \\ 4Pr^{-1} + (\phi\vartheta)' = 0 \end{aligned}\right\} \tag{29}$$

where

$$\left.\begin{aligned} &\phi' = \frac{\partial\phi}{\partial\eta}, \quad \vartheta' = \frac{\partial\vartheta}{\partial\eta}, \quad u = \frac{\partial\psi}{\partial y}, \quad v = -\frac{\partial\psi}{\partial x}, \\ &\psi = (b\bar{Q}\nu x/c_p\rho^2)^{1/4}\phi(\eta), \\ &\vartheta = (\bar{Q}/\rho c_p)^{3/4}(\rho/b\nu x)^{1/4}\vartheta(\eta), \\ &\eta = (y/\nu x)^{3/4}(b\bar{Q}/\rho^2 c_p)^{1/4}, \\ &u = (b\bar{Q}/c_p\nu x\rho^2)^{1/2}u(\eta). \end{aligned}\right\} \tag{30}$$

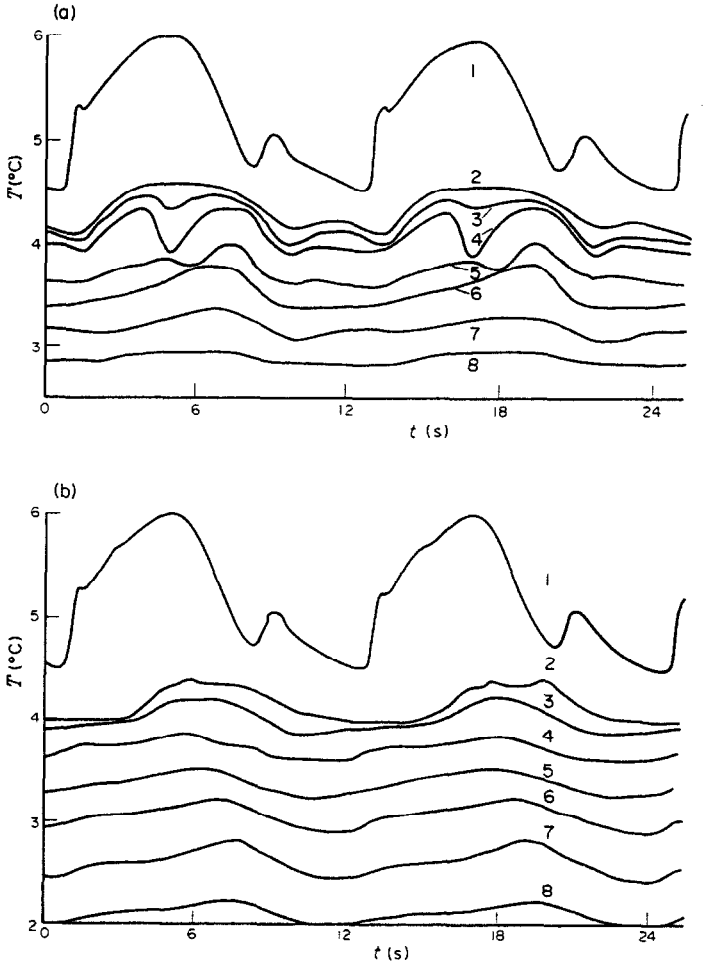

FIG. 23. Temperature variations in time for different values of y at $t_0 = 12$ s. (a) 1, $y = 0$, $x = 1.5$ mm, $x = 9$ mm; 2, $y = 0.2$ mm; 3, $y = 0.36$ mm; 4, $y = 1.17$ mm; 5, $y = 1.7$ mm; 6, $y = 2.58$ mm; 7, $y = 3.46$ mm; 8, $y = 4.55$ mm. (b) 1, $y = 0$, $x = 1.5$ mm, $x = 25$ mm; 2, $y = 0.14$ mm; 3, $y = 0.7$ mm; 4, $y = 1.7$ mm; 5, $y = 2.77$ mm; 6, $y = 4.26$ mm; 7, $y = 6.08$ mm; 8, $y = 8.56$ mm.

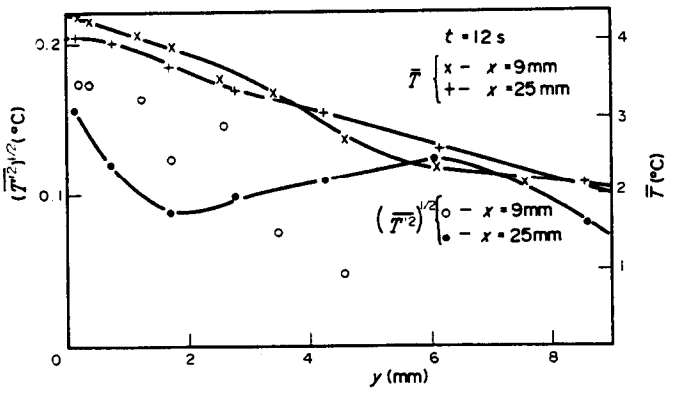

FIG. 24. The mean values $\bar{T}$ and mean-square temperature fluctuations over the layer depth ($t_0 = 12$ s).

Physically, boundary conditions (28) cannot be realized for the outer part of the boundary layer in a steady flow, as testified by the experimental investigations described above. Mathematically, it is necessary to prove whether or not the solution to equation (29) exists under boundary conditions (4) and (28).

Boundary conditions (28) for $y \gg \delta (y \to \infty)$ have a common feature with actual conditions (6), lying on the fact that in actual conditions the heat flux is also

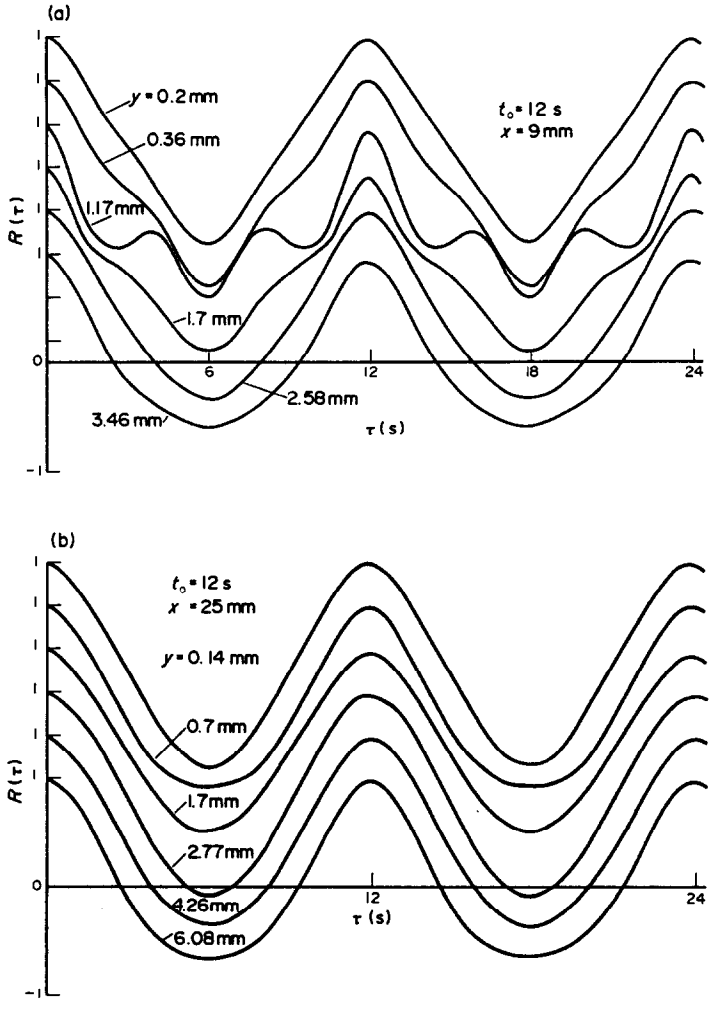

FIG. 25. The autocorrelation functions of temperature fluctuations over the layer depth ($t_0 = 12$ s). (a) $x = 9$ mm. (b) $x = 25$ mm.

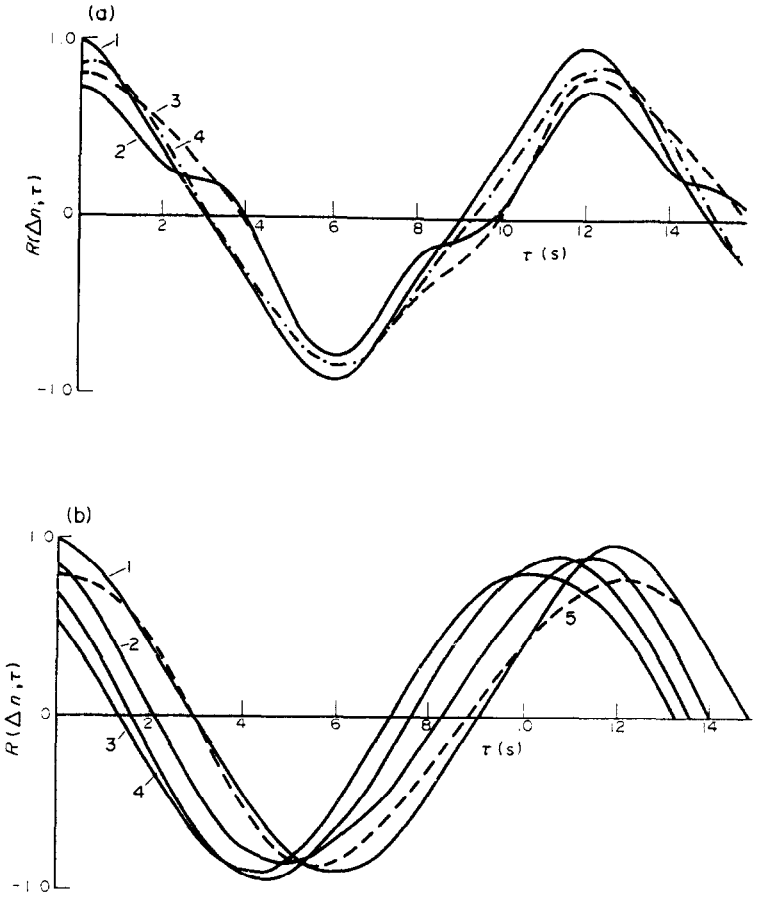

FIG. 26. The space–time correlation functions of temperature fluctuations over the layer depth for different shifts $\Delta n(t_0 = 12$ s). (a) $x = 9$ mm, $\Delta n = (y-0.2)$ mm: 1, $y = 0.2$ mm; 2, $y = 0.66$ mm; 3, $y = 1.7$ mm; 4, $y = 4.55$ mm. (b) $x = 25$ mm, $\Delta n = (y-0.14)$ mm: 1, $y = 0.14$; 2, $y = 0.7$ mm; 3, $y = 1.7$ mm; 4, $y = 2.77$ mm; 5, $y = 8.56$ mm.

absent at the edge of the boundary layer. The difference consists of the fact that at the edge of the boundary layer in the boundary-value problem considered $v = v_n = \text{const.}$, T varies by law (6) and, therefore, the self-similar solution (30) does not exist for the 'outer part' of the boundary layer.

It is assumed that the velocity of the periodic flow propagation is comparable with that of the liquid motion on the free surface at $\bar{Q} = \text{const.}$

$$u \sim \left(\frac{b\bar{Q}}{c_p x v \rho^2}\right)^{1/2} \tag{31}$$

then

$$x_0 \sim u_0 t_0 \sim t_0 \left(\frac{b\bar{Q}}{c_p x_p v \rho^2}\right)^{1/2} \tag{32}$$

and

$$x_0(\rho^2 v c_p / b\bar{Q} t_0^2)^{1/3} = \text{const.} \tag{33}$$

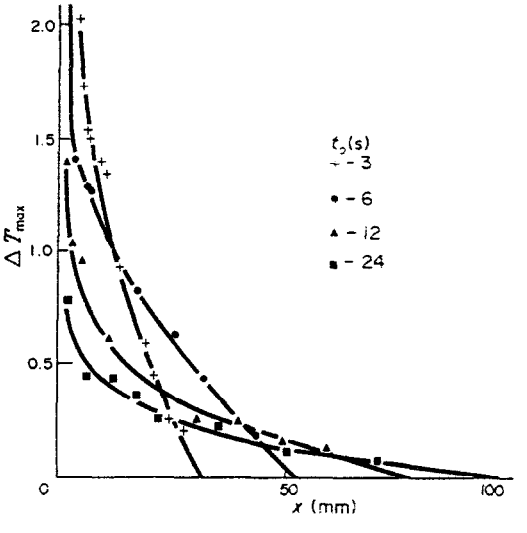

FIG. 27. The amplitude (ΔT_{max}) of periodic temperature fluctuations on the free surface vs 'x'.

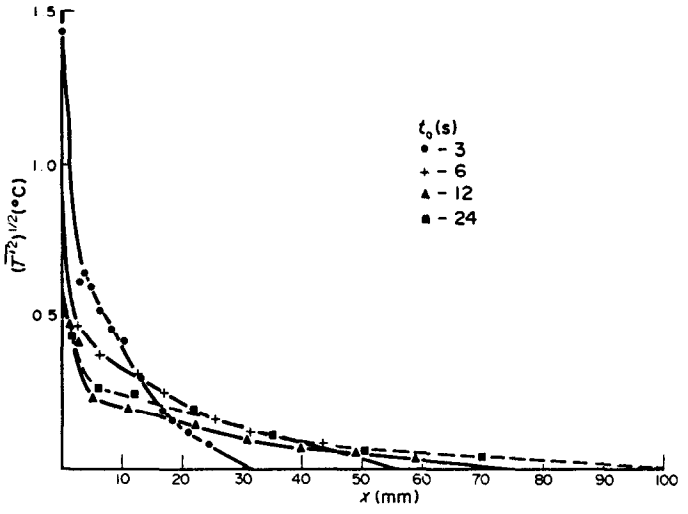

FIG. 28. The mean-square temperature on the free surface vs 'x'.

Figures 27 and 28 give the amplitudes of the periodic disturbances and mean-square temperature fluctuations along the free surface for different values of t_0. The damping length for the periodic disturbances x_0 is determined from Figs. 27 and 28 from the intersection of the averaging curves with the x-axis.

As in the case of the propagation of periodic flows in a plane layer [1], relation (33) is confirmed within experimental accuracy for $t_0 = 3$–24 s

$$x_0(\rho\mu c_p/b\bar{Q}t_0^2)^{1/3} = 1.5. \quad (34)$$

For a larger volume, the value of the above criterion (34) is somewhat lower than for the plane layer. This can be attributed to the high velocity of the averaged free surface flow in the plane layer [1].

The distribution of periodic flows at the free surface of ethyl alcohol is mainly determined by thermocapillary forces. Due to a large inertia for frequencies higher than 1/24 Hz, the thermal gravitational flows do not exert an appreciable effect on the damping length of periodic flows (x_0). On the other hand, the steady flows are governed by the interaction between the thermocapillary and thermogravitational forces. It should be expected that far from the heater, at large values of x, the thermogravitational forces will become predominant with a decrease in the gradient $|\partial T/\partial x|_0$.

REFERENCES

1. A. G. Kirdyashkin, Thermocapillary periodic flows, *Int. J. Heat Mass Transfer* **30**, 109–124 (1985).
2. A. G. Kirdyashkin, Thermogravitational and thermocapillary flows in a horizontal liquid layer under the condition of a horizontal temperature gradient, *Int. J. Heat Mass Transfer* **27**, 1205–1218 (1984).
3. V. D. Zimin, Yu. N. Lyakhov and M. P. Sorokin, Convection in a vertical cylinder heated from below, *Hydrodynamics (Perm)* No. 1, 73–84 (1975).

ECOULEMENTS THERMOCAPILLAIRES PERMANENTS ET PERIODIQUES DANS UNE COUCHE HORIZONTALE BEAUCOUP PLUS EPAISSE QUE LA COUCHE LIMITE A LA SURFACE LIBRE

Résumé—On présente les résultats d'une étude expérimentale sur les écoulements thermocapillaires et thermogravitationnels dans une couche horizontale beaucoup plus épaisse que la couche limite hydrodynamique à la surface libre. Il y a une source de chaleur linéique sous la surface libre et un puits thermique sur les faces verticales opposées. Pour un flux thermique constant, des couches limites se développent sur la surface libre horizontale et sur les faces verticales froides. On présente des profils de vitesse et de température mesurés dans les couches limites. Des solutions analytiques sont obtenues. Les configurations des écoulements périodiques thermocapillaires étudiées pour des périodes inférieures à 24 s concernent ; les températures instantanées et moyennes, les valeurs moyennes et instantanées du coefficient de frottement à la surface libre, la variance des fluctuations de température, les fonctions de corrélation espace–temps et les limites de la propagation des écoulements périodiques.

STETIGE UND PERIODISCHE THERMOKAPILLARE STRÖMUNGEN IN EINER HORIZONTALEN FLUIDSCHICHT, DEREN DICKE SEHR VIEL GRÖSSER ALS DIE GRENZSCHICHT AN DER FREIEN OBERFLÄCHE IST

Zusammenfassung—In dieser Arbeit werden die Ergebnisse einer experimentellen Untersuchung von thermokapillaren und auftriebsbedingten Strömungen in einer horizontalen Fluidschicht vorgestellt, deren Dicke sehr viel größer als die der hydrodynamischen Grenzschicht an der freien Oberfläche ist. Unterhalb der freien Oberfläche befindet sich eine lineare Wärmequelle, an der gegenüberliegenden senkrechten Wand eine Wärmesenke. Bei konstanter Wärmestromdichte bilden sich Grenzschichten entlang der horizontalen freien Oberfläche und der senkrechten Kühlfläche aus. Die in den Grenzschichten gemessenen Geschwindigkeits- und Temperaturprofile werden dargestellt. Die Grenzschicht an der Kühlfläche sowie der Bereich außerhalb der Grenzschicht wird analytisch berechnet. Die Form der periodischen thermokapillaren Strömungen mit einer Periodendauer kleiner als 24 s wird untersucht. Dabei werden folgende Größen bestimmt: die momentanen und die zeitlich gemittelten Temperaturen, die momentanen und die zeitlich gemittelten Werte des Reibungskoeffizienten an der freien Oberfläche, die Varianz der Temperaturschwankungen, die zeitlich–räumlichen Korrelationsfunktionen und die Grenzen der Ausbreitung der periodischen Strömungen.

ТЕРМОКАПЛЛЯРНЫЕ СТАЦИОНАРНЫЕ И ПЕРИОДИЧЕСКИЕ ТЕЧЕНИЯ В ГОРИЗОНТАЛЬНОМ СЛОЕ, МНОГО БОЛЬШЕМ ТОЛЩИНЫ ПОГРАНИЧНОГО СЛОЯ У СВОБОДНОЙ ПОВЕРХНОСТИ

Аннотация—В статье излагаются результаты экспериментальных исследований термокапиллярных и термогравитационных течений в горизонтальном слое, много большем толщины гидродинамического пограничного слоя у свободной поверхности. Линейный источник тепла расположен под свободной поверхностью, охлаждение—у вертикального противоположного торца. При постоянном тепловом потоке организуются пограничные слои у свободной горизонтальной и охлаждающей вертикальной поверхности. Представлены измерения профилей скорости и температуры в пограничных слоях. Получены аналитические решения для пограничного слоя у охлаждающей поверхности и вне пограничных слоев. Исследуется структура периодических термокапиллярных течений при периодах, меньших 24 с: актуальные и средние значения температуры, актуальные и средние значения коэффициента трения у свободной поверхности, дисперсия пульсации температуры, пространственно–временные корреляционные функции, границы распространения периодических течений.